Published in final edited form as:
Arch Biochem Biophys. 2008 September 1; 477(1): 105–112. doi:10.1016/j.abb.2008.04.032.

SOD-like activity of Mn(II) *β*-octabromo-*meso*-tetrakis(*N*-methylpyridinium-3-yl)porphyrin equals that of the enzyme itself

Gilson DeFreitas-Silva[1], **Júlio S. Rebouças**[2], **Ivan Spasojevi**[3], **Ludmil Benov**[4], **Ynara M. Idemori**[1,*], and **Ines Batini -Haberle**[2,*]

1 *Departamento de Química, ICEx, Universidade Federal de Minas Gerais, Belo Horizonte, MG 31270-901, Brazil*

2 *Department of Radiation Oncology, Duke University Medical School, Durham, NC 27710, USA*

3 *Department of Medicine, Duke University Medical School, Durham, NC 27710, USA*

4 *Department of Biochemistry, Faculty of Medicine, Kuwait University, Safat, 13110, Kuwait*

Abstract

Mn porphyrins are among the most efficient SOD mimics with potency approaching that of SOD enzymes. The most potent ones, Mn(III) *N*-alkylpyridylporphyrins bear positive charges in a close proximity to the metal site, affording thermodynamic and kinetic facilitation for the reaction with negatively charged superoxide. The addition of electron-withdrawing bromines onto *β*-pyrrolic positions dramatically improves thermodynamic facilitation for the $O_2^{\bullet-}$ dismutation. We have previously characterized the *para* isomer, $Mn^{II}Br_8TM\text{-}4\text{-}PyP^{4+}$ [Mn(II) *β*-octabromo-*meso*-tetrakis (*N*-methylpyridinium-4-yl)porphyrin]. Herein we fully characterized its *meta* analogue, $Mn^{II}Br_8TM\text{-}3\text{-}PyP^{4+}$ with respect to uv/vis spectroscopy, electron spray mass spectrometry, electrochemistry, $O_2^{\bullet-}$ dismutation, metal-ligand stability, and the ability to protect SOD-deficient *E. coli* in comparison with its *para* analogue. The increased electron-deficiency of the metal center stabilizes Mn in its +2 oxidation state. The metal-centered Mn^{III}/Mn^{II} reduction potential, $E_{½}$ = + 468 mV *vs* NHE, is increased by 416 mV with respect to non-brominated analogue, $Mn^{III}TM\text{-}3\text{-}PyP^{5+}$ and is only 12 mV less positive than for *para* isomer. Yet, the complex is significantly more stable towards the loss of metal than its *para* analogue. As expected, based on the structure-activity relationships, a large increase in $E_{½}$ results in exceptionally high catalytic rate constant for the $O_2^{\bullet-}$ dismutation, log $k_{cat} \geq 8.85$; 1.5-fold increase with respect to the *para* isomer. The IC_{50} was calculated to be ≤ 3.7 nM. Manipulation of the electron-deficiency of a cationic porphyrin resulted, therefore, in the highest k_{cat} ever reported for a metalloporphyrin, being essentially identical to the k_{cat} of superoxide dismutases (log k_{cat} = 8.84 – 9.30). The positive kinetic salt effect points to the unexpected, unique and first time recorded behavior of Mn β-octabrominated porphyrins when compared to other Mn porphyrins studied thus far. When species of opposing charges react, the increase in ionic strength invariably results in the decreased rate constant; with brominated porphyrins the opposite was found to be true. The effect is 3.5 - fold greater with *meta* than with *para* isomer, which is discussed with respect to the closer proximity of the quaternary nitrogens of the *meta* isomer to the metal center than that of the *para* isomer. The potency of $Mn^{II}Br_8TM\text{-}3\text{-}PyP^{4+}$ was corroborated by *in vivo* studies, where 500 nM allows SOD-deficient *E. coli* to grow ≥ 60% of the growth of wild type; at concentrations ≥5 μM it exhibits toxicity. Our work shows that exceptionally high k_{cat} for the $O_2^{\bullet-}$ disproportionation can be achieved not only with an N_5-type

*Corresponding authors: Ynara Marina Idemori, Ph. D., Departamento de Química, ICEx, Universidade Federal de Minas Gerais, Av. Antônio Carlos, 6627, Pampulha, Belo Horizonte, MG, 31270-901, Brazil., Tel: +55-31-3499-5762, Fax: +55-31-3499-5700, e-mail: ynara@ufmg.br, Ines Batinic-Haberle, Ph. D., Department of Radiation Oncology-Cancer Biology, Duke University Medical Center, Research Drive, 281b/285 MSRB I, Box 3455, Durham, NC 27710, Tel: 919-684-2101, Fax: 919-684-8718, e-mail: ibatinic@duke.edu.

coordination motif, as rationalized previously for aza crown ether (cyclic polyamines) complexes, but also with a N_4-type motif as in the Mn porphyrin case; both motifs sharing “up-down-up-down” steric arrangement.

Keywords

SOD-mimics; Mn porphyrin; Mn(II) *β*-octabromo-*meso*-tetrakis-(*N*-methylpyridinium-3-yl) porphyrin; $Mn^{II}Br_8TM\text{-}3\text{-}PyP^{4+}$; SOD-deficient *E. coli*

Introduction

Superoxide ($O_2^{\bullet-}$) is involved in a variety of pathological and physiological processes. Under pathological conditions the endogenous superoxide dismutases may not efficiently remove the excessive $O_2^{\bullet-}$ produced; therefore there is a need for low-molecular weight SOD mimics. We have been developing Mn porphyrin-based SOD mimics for over a decade. We have established structure activity relationship (SAR) for both Mn and Fe porphyrins [1] between the metal-centered redox potential and the rate constant for $O_2^{\bullet-}$ dismutation and refined it recently to account for the differently charged/sized Mn porphyrins [2–5]. The introduction of both electron-withdrawing groups and positive charges onto the porphyrin core affords thermodynamic and kinetic/electrostatic facilitation for the approach of superoxide to the redox-cycling metal site [1–4]. The higher the metal-centered reduction potential the higher is the ability of the metalloporphyrin to catalyze $O_2^{\bullet-}$ dismutation. Additionally, the ability of Mn porphyrins to eliminate peroxynitrite was found to parallel the $O_2^{\bullet-}$ dismuting activity [6] and is, therefore, governed by closely related SAR. Moreover, as a result of the easy reducibility of the potent SOD mimics, their action *in vivo* may be coupled to cellular reductants (ascorbic acid, tetrahydrobiopterin, less efficiently with glutathione), converting their function to superoxide or $ONOO^-$ reductases [6–11].

In addition to the SAR we used SOD-deficient *E. coli* as a very convenient and valuable tool for evaluating the *in vivo* ability of the metalloporphyrin to substitute for the native SOD enzyme. Based on *E. coli* studies we can then predict the therapeutic usefulness of metalloporphyrins. In all cases tested Fe porphyrins killed *E. coli* therefore in our further studies we focused predominantly on Mn porphyrins.

Our very first compound that proved the validity of our approach was the electron-deficient Mn(II) *β*-octabromo-*meso*-tetrakis(*N*-methylpyridinium-4-yl)porphyrin, $Mn^{II}Br_8TM\text{-}4\text{-}PyP^{4+}$ (Fig. 1), that has the log k_{cat} = 8.34 and $E_{½}$ = +480 mV *vs* NHE [12] and is protective to *E. coli* at nM levels. Our further synthetic efforts in searching for a potential therapeutic based on the SAR led us to Mn(III) *ortho N*-alkylpyridylporphyrins as the most potent candidates for forwarding them into animal models where superoxide-mediated damage is involved. Thus remarkable effects were observed in cancer, radiation, diabetes, ALS, Alzheimer’s disease etc [13–23]. Further, along with our mechanistic studies we observed a dramatic impact of the positive charges of the Mn porphyrin on the $O_2^{\bullet-}$ dismutation; the rate constants are more than two orders of magnitude higher when compared to the neutral or negatively charged porphyrins [3,4]. Thus, $Mn^{III}TE\text{-}2\text{-}PyP^{5+}$ is 130-fold more potent SOD mimic than its singly charged $Mn^{III}Br_8T\text{-}2\text{-}PyP^{+}$ [3], and 400-fold more potent than its negatively charged analogue $[Mn^{III}Br_8TSPP]^{3-}$ [4]. Charge distribution had also remarkable impact [2]. In summary both metal-centered redox potential and charges in close proximity to the metal site have a major impact on the antioxidant potency of the Mn porphyrin. As our knowledge on porphyrins increases it became obvious that another major factor is their *in vivo* availability [2,4,24,25]. *The optimal combination of thermodynamics, kinetics, bioavailability and low toxicity will determine the best drug candidate.*

Our first report on a potent *ortho* isomer, Mn^{III}TM-2-PyP^{5+}, in protecting SOD-deficient *E. coli* indicated that the *meta* isomer, Mn^{III}TM-3-PyP^{5+}, although ~10-fold inferior with respect to *in vitro* antioxidant potency [1] may still be effective *in vivo* [26]. Indeed, *meta* isomer was comparable to the *ortho* analogue in providing protection to SOD-deficient *E. coli* to grow aerobically in restricted five amino acid-medium while *para* isomer, MnTM-4-PyP^{5+}, was toxic [26]. The reason likely lies in lesser bulkiness of the *meta* isomer, which allows it to accumulate within *E. coli* at higher levels than the *ortho* analogue [26]. *Para* isomer was toxic due to its interactions with nucleic acids [26]. Guided by these collective *in vitro*, *in vivo*, and SAR results [1–5,12,24–26], we resumed herein our studies on the *meta* Mn(III) *N*-alkylpyridylporphyrins by preparing a brominated derivative of Mn^{III}TM-3-PyP^{5+}. This is the first report on the synthesis and characterization of $Mn^{II}Br_8$TM-3-PyP^{4+} (Fig. 1). We also compared its *in vitro* and *in vivo* properties to those of the *para* analogue, $Mn^{II}Br_8$TM-4-PyP^{4+} (Fig. 1) [12]. The synthesis of an *ortho* analogue, for mechanistic purposes, has not been achieved as its electron-deficiency would likely preclude the existence of a Mn complex stable enough for isolation and characterization.

Experimental

Materials

Meso-tetrakis(*N*-methylpyridinium-3-yl)porphyrin (chloride salt) was purchased from MidCentury Chemicals (Chicago, IL) and used as received. Mn^{III}TM-2-PyP^{5+} (chloride salt) [26] and Mn^{III}TM-3-PyP^{5+} (chloride salt) [26] were prepared and characterized as previously described.

Xanthine and equine ferricytochrome *c* (lot no. 7752 [27,28]) were from Sigma, whereas xanthine oxidase was prepared by R. Wiley [29] and was a gift from K.V. Rajagopalan.

$MnCl_2 \cdot 4H_2O$ and $CuCl_2 \cdot 2H_2O$ were purchased from J. T. Baker and Aldrich, respectively. Anhydrous *N*,*N*-dimethylformamide (DMF, Sigma-Aldrich Chemical Co) was kept over 4 Å molecular sieves. Bromine and NaCl were from Aldrich, whereas ethyl ether (anhydrous), acetone, and 2-propanol were from EMD. Methanol was from Mallinckrodt. All other chemicals and solvents were of analytical grade and used without further purification.

Methods

Spectral analyses

The uv/vis measurements were performed using a Shimadzu UV-2501PC spectrophotometer at 0.5 nm resolution. The elemental analyses were conducted by Atlantic Microlabs (Norcross, GA, USA).

The mass spectrometric (ESI: electrospray ionization) measurements were performed on an Applied Biosystems MDS Sciex 3200 Q Trap liquid chromatography/MS/MS spectrometer at the Duke Comprehensive Cancer Center, Shared Resources. All porphyrins were analyzed using 1:1 acetonitrile:water solutions, at 20 and 30 V cone voltages as described previously [11,27].

Electrochemistry

The cyclic voltammetry was carried out on a CH Instruments Model 600 Voltammetry Analyzer [1]. A three-electrode system consisted of a 3 mm-diameter glassy carbon button working electrode (Bioanalytical Systems), the Ag/AgCl reference electrode, and a Pt auxiliary electrode was used in a small volume cell (3.0 mL). Helium-purged solutions contained 0.05 M phosphate buffer (pH 7.8), 0.1 M NaCl, and 0.5 mM metal-free porphyrin or Mn porphyrin.

The scan rates were 0.01–0.5 V s^{-1}, typically 0.1 V s^{-1}. The potentials were standardized against Mn^{III}TE-2-PyP^{5+} (chloride salt) ($E_{½}$ = +228 mV *vs* NHE [1]). Also another experiment was done where the voltammogram was measured first in 0.09 M phosphate buffer only, then solid NaCl was added to yield a 0.1 M Cl^- concentration and the voltammogram was recorded again. This was devised to assess the possible chloride binding to the Mn porphyrin axial site.

Synthesis of *β*-octabromo-*meso*-tetrakis(*N*-methylpyridinium-3-yl)porphyrinato-manganese (II) chloride, $Mn^{II}Br_8$TM-3-$PyPCl_4$

This fully *β*-brominated complex was prepared from H_2TM-3-PyP^{4+} in four steps. The first three steps were based on the synthetic protocol reported by *Richards et al* [30] for the synthesis of *para*-isomer (H_2TM-4-PyP^{4+}) derivatives.

First, Cu^{II}TM-3-$PyPCl_4$ was prepared by the metallation of H_2TM-3-$PyPCl_4$ (67.1 mg, 0.0818 mmol) with $CuCl_2$:$2H_2O$ (109 mg, 0.638 mmol) in a CH_3OH:H_2O mixture (10:1, 12 mL) at 45°C. After 1 hour, the volume was reduced to approximately 5 mL in a rotavapor and 5 mL of 2-propanol was added to precipitate the copper porphyrin. The solid was filtrated, washed with 2-propanol until the washings were colorless, and dried under vacuum at room temperature. This compound was carried forward to bromination (second step) without further purification. A Br_2 (0.2 mL, 4 mmol) solution in DMF (2 mL) was added dropwise over 30 minutes to a well-stirred solution of Cu^{II}TM-3-PyP^{4+} (72.1 mg, 0.0818 mmol) in DMF (8 mL) at room temperature. The color of the solution changed immediately from red to green. The reaction course was monitored by uv/vis and by TLC (silica gel, 1:1:8 saturated aqueous KNO_3:H_2O:MeCN mixture as eluent). After 48 hours the reaction was quenched by the addition of approximately 5 mL of water, which precipitated the brominated compound. The copper brominated porphyrin was collected by filtration and washed first with water (3 × 3 mL) then with 3 mL of a 1:1 etanol:2-propanol mixture (excess Br_2 in the filtrate can be quenched by sodium metabisulfite prior to disposal). The green powder was air-dried and then dissolved in a minimal amount of water. The copper porphyrin was precipitated as the PF_6^- salt by the addition of a concentrated aqueous solution of NH_4PF_6. The precipitate was filtered off, thoroughly washed with diethyl ether, and air-dried. The resulting solid was then dissolved in acetone and re-precipitated as the chloride salt by the addition of saturated tetrabutylammonium chloride solution in acetone. The $Cu^{II}Br_8$TM-3-$PyPCl_4$ complex was washed thoroughly with acetone and dried under vacuum at room temperature. Yield: 65 mg (53 % based on starting H_2TM-3-PyP^{4+}). Uv/vis (0.05 M phosphate buffer, pH 7.8): 266.0 nm (ε/M^{-1} cm^{-1}, 15,239), 378.5 (13,686), 447.0 (55,239), 472.5 (sh; 35,405), 588.0 (7,526). ESI-MS (1:1, H_2O:MeCN): clusters centered at *m/z* 343.2 ($Cu^{II}Br_8$TM-3-PyP^{4+}/4) and *m/z* 469.4 ([$Cu^{II}Br_8$TM-3-PyP^{4+} + Cl^-]$^{3+}$/3).

In the third step, the $Cu^{II}Br_8$TM-3-PyP^{4+} complex (45.6 mg, 0.0301 mmol) was demetallated by the slow addition of a concentrated sulfuric acid (6.0 mL, 111 mmol) while cooled to 10° C. Upon dissolution, the color of the reaction mixture changed immediately from green to greenish orange; cooling was discontinued and the reaction mixture was allowed to reach the room temperature. The acid solution was left under stirring at room temperature for 4 hours, after which it was carefully poured over the ice (~64 g). Once the ice melted the octabrominated free-base porphyrin was precipitated as the PF_6^- salt by the addition of a concentrated $NH_4PF_{6\,(aq)}$ solution. The precipitate was recovered by filtration, washed first with water (2 × 3 mL) then with a 1:1 diethyl ether:2-propanol mixture (5 mL), and air-dried. The resulting solid was then dissolved in acetone and precipitated as the chloride salt by the addition of saturated tetrabutylammonium chloride solution in acetone as with $Cu^{II}Br_8$TM-3-PyP^{4+} to yield the corresponding free-base. Yield: 41.5 mg (95 % based on starting $Cu^{II}Br_8$TM-3-PyP^{4+}). Anal. Calcd for H_2Br_8TM-3-$PyPCl_4$·$9H_2O$, $C_{44}H_{48}Br_8N_8O_9Cl_4$: C, 32.74; H, 3.00; N, 6.94. Found: C, 32.66; H, 3.03; N, 6.84. Uv/vis (0.05 M phosphate buffer, pH 7.8): 270.5

nm (ε/M^{-1} cm^{-1}, 26,351), 508.0 (95,663), 646.0 (6,375), 729.0 (8,104). ESI-MS (1:1, H_2O:MeCN): clusters centered at *m/z* 328.0 ($H_2Br_8TM\text{-}3\text{-}PyP^{4+}$/4) and m/z 436.8 ([$H_2Br_8TM\text{-}3\text{-}PyP^{4+}$ + e^-]$^{3+}$/3).

In the last step the $Mn^{II}Br_8TM\text{-}3\text{-}PyP^{4+}$ was synthesized using a procedure adapted from that described for the *para*-isomer $Mn^{II}Br_8TM\text{-}4\text{-}PyP^{4+}$ [12]. $H_2Br_8TM\text{-}3\text{-}PyP^{4+}$ (38.3 mg, 0.0264 mmol) was dissolved in 10 mL of water and the pH was then raised to 11.2 by the addition of ~30μL of 1 M NaOH. This increase in pH was accompanied by a color change from green to reddish pink. A 2-fold excess of $MnCl_2{\cdot}4H_2O$ (10.5 mg, 0.0528 mmol) was added followed by a drop in pH from 11.2 to ~9 along with instantaneous color change from reddish pink to green. Metathesis of the anions of this Mn porphyrin with NH_4PF_6 to yield the PF_6^- salt, and subsequently with tetrabutylammonium chloride in acetone to yield the chloride salt of $Mn^{II}Br_8TM\text{-}3\text{-}PyP^{4+}$ was carried out as with $Cu^{II}Br_8TM\text{-}3\text{-}PyP^{4+}$. Yield: 36.6 mg (92 % based on starting $H_2Br_8TM\text{-}3\text{-}PyP^{4+}$). Anal. Calcd for $Mn^{II}Br_8TM\text{-}3\text{-}PyPCl_4{\cdot}5H_2O{\cdot}NH_4PF_6$, $C_{44}H_{42}Br_8N_9O_5Cl_4PF_6Mn$: C, 30.06; H, 2.41; N, 7.17. Found: C, 29.82; H, 2.86; N, 7.43. Uv/vis (0.05 M phosphate buffer, pH 7.8): 265.5 nm (ε/M^{-1} cm^{-1}, 31,689), 415.5 (34,248), 483.0 (84,693), 599.0 (10,053). ESI-MS (1:1, H_2O:MeCN): clusters centered at *m/z* 340.7 ($Mn^{II}Br_8TM\text{-}3\text{-}PyP^{4+}$/4) and at m/z 465.5 ([$Mn^{II}Br_8TM\text{-}3\text{-}PyP^{4+}$ + Cl^-]$^{3+}$/3). Of note, when a 20-fold excess of Mn was used, as in the standard metallation procedure for the non-brominated analogues [26], the pH dropped too much (to ~6.5), due to the extensive hydrolysis of Mn, and prevented a completion of metallation.

Superoxide Dismutase Activity

The catalytic rate constants for the $O_2^{\bullet-}$ disproportionation were determined by the cytochrome *c* (cyt *c*) assay [31,32]. We have previously compared the k_{cat} determined by pulse radiolysis and with cyt c assay for several of our Mn porphyrins and $MnCl_2$ [27,32]. The k_{cat} determined by both methods were the same, which justified using a convenient cyt c assay for testing our prospective SOD mimics. The xanthine/xanthine oxidase (40 μM xanthine, ~2 nM xanthine oxidase) was the source of $O_2^{\bullet-}$and ferricytochrome *c* was used as the indicating scavenger of $O_2^{\bullet-}$. The reduction of cyt *c* was followed at 550 nm. Assays were conducted in 0.05 M phosphate buffer, pH 7.8 in the presence and absence of 0.1 mM EDTA to account for any metal impurity. A 2μM Mn porphyrin stock solution (in 0.05 M phosphate buffer, pH 7.8) was made without EDTA and allowed to reach the metal/ligand equilibrium (~10 min), after which the solution was used for cyt c assay (see Fig. 2 bellow). Rate constants for the reactions of Mn porphyrins with $O_2^{\bullet-}$ were based upon the competition with 10 μM cyt *c*, $k_{cyt\ c} = 2.6 \times 10^5$ M^{-1} s^{-1} [31,32]. The $O_2^{\bullet-}$ was produced at 1.2 μM min^{-1}. Any possible interference of Mn porphyrins with production of $O_2^{\bullet-}$ was examined following urate formation at 295 nm in the absence of cyt *c*. No reoxidation of cytochrome *c* by metalloporphyrins was observed. The effect of ionic strength upon the rate constant of dismutation was determined as above using either NaCl (in the range of 0 to 0.10 M) or phosphate (in the range of 0.05 to 0.087 M) as ionic strength modifier. All measurements were done at (25 ± 1)°C and unaffected by the presence or absence of 15 μg mL^{-1} catalase.

We have previously observed that the SOD-like activity of the *para* isomer $Mn^{II}Br_8TM\text{-}4\text{-}PyP^{4+}$ was the same with or without EDTA [12]. We confirmed such an observation in this work and verified that the SOD activity of $Mn^{II}Br_8TM\text{-}3\text{-}PyP^{4+}$ is also unaffected by the presence or absence of EDTA in the assay, if EDTA was added into the cuvette about the time the cyt *c* reduction was to be followed at 550 nm. When EDTA was added to the $Mn^{II}Br_8TM\text{-}3\text{-}PyP^{4+}$ stock solution a considerable loss of Mn during the collection of data affected significantly the consistency in k_{cat} determination.

The SOD activity of metal-free ligand was assessed also. The 5 μM stock solution was made with 1 mM EDTA in the 0.05 M phosphate buffer; EDTA was added to prevent any metallation that could otherwise occur with traces of metals present in the solution.

Based on the linear relationship between the $E_{1/2}$ (Mn^{III}/Mn^{II}) and the acidity of the inner pyrrolic nitrogens [1], the slightly less positive $E_{1/2}$ of the β-octabrominated Mn porphyrin ($Mn^{II}Br_8TM\text{-}3\text{-}PyP^{4+}$, see below) indicates that the pK_{a2} of the free base *meta* isomer is only slightly higher than the pK_{a2} = 6.5 of the *para* isomer [30] (pK_{a2} relates to the equilibrium: $H_2P^{4+} = HP^{3+} + H^+$). Consequently, there may be < 10% of the diprotonated species ($H_2Br_8TM\text{-}3\text{-}PyP^{4+}$) present at pH 7.8. Thus, in all experiments performed at pH 7.8, we assumed that the $HBr_8TM\text{-}3\text{-}PyP^{3+}$ is the major species in solution.

E. coli growth experiments

Escherichia coli strains used in this study were AB1157, wild type (*F-thr-1; leuB6; proA2; his-4; thi-1; argE2; lacY1; galK2; rpsL; supE44; ara-14; xyl-15; mtl-1; tsx-33*), and JI132, SOD-deficient, *sodA*$^-$*sodB*$^-$ (same as AB1157 plus (*sodA::mudPR13*)25 (*sodB-kan*)1-Δ2). Both strains were obtained from J. A. Imlay [33]. The experiments were carried out as described in detail by Rebouças *et al* [2]. Briefly, cultures were grown aerobically in a five-amino acid medium in 96-well flat-bottom microtiter plates [34] on a thermostatic shaker at 37°C and 200 rpm. Approximately 1 mM stock solutions of brominated porphyrins were prepared immediately before the start of the experiment, and the exact concentration determined by uv/vis spectroscopy. They were then diluted to μM solutions which were added to the medium. The effect of metal-free porphyrin, Mn porphyrins, and $MnCl_2$ on the growth of these strains was followed turbidimetrically at 700 nm (to minimize the interference of the compounds studied) and compared to the growth curves of both strains in the absence of these compounds (controls). Three experiments were performed and the data from a representative one are shown herein.

Results and Discussion

In order for a Mn porphyrin to be an efficient SOD mimic, its reduction potential should be around the midway between the potential for the reduction and oxidation of $O_2^{\bullet-}$, *i.e.* ~ +300 mV as is the case with the enzymes themselves [35–37]. Unsubstituted Mn(III) porphyrins are stable in Mn +3 oxidation state thus can not oxidize $O_2^{\bullet-}$ in the first step of a catalytic cycle of a $O_2^{\bullet-}$ dismutation process. The increase in the electron-deficiency of the Mn(III) porphyrin by introducing electron-withdrawing groups on its core results in an increased metal-centered reduction potential, stabilizes the Mn +2 oxidation state, and thus makes Mn(III) porphyrins more readily reducible by $O_2^{\bullet-}$. That in turn leads to the increase in catalytic rate constants for $O_2^{\bullet-}$dismutation as described by structure-activity relationships [1,2,4]. The most potent porphyrins that have the $E_{1/2}$ around the midway potential for the $O_2^{\bullet-}$ reduction and oxidation have equal thermodynamic facilitation for both half-reactions (Equations 1 and 2) of the catalytic cycle.

$$Mn^{III}P^{5+} + O_2^{\bullet-} = Mn^{II}P^{4+} + O_2 \quad k_{red} \tag{1}$$

$$Mn^{II}P^{4+} + O_2^{\bullet-} + 2H^+ = Mn^{III}P^{5+} + H_2O_2 \quad k_{ox} \tag{2}$$

Consequently, the k_{ox} and k_{red} are nearly identical as is the case with SOD enzymes [38,39] themselves, and with our porphyrins [3,40]. As the redox potential increases further the oxidation of Mn(II) porphyrin becomes rate-limiting step, as is the cases with octabrominated porphyrins, leading eventually to a drop in k_{cat}; a bell-shaped curve in the k_{cat} *vs* $E_{½}$ plot is observed [2,4,41].

We have further shown that the placement and distribution of charges close to the metal site are other major factors contributing to the SOD-like potency of Mn porphyrins [2–4]. Finally, the appropriate lipophilicity and the size would greatly impact the *in vivo* activity of these compounds [11,24].

We have shown that *ortho* isomers of Mn(III) alkylpyridylporphyrins have thus far been the most potent porphyrinic compounds *in vitro*, with log k_{cat} being as high as 8.60 [42], and have proven remarkably effective *in vivo* [41]. Whereas *ortho*, *meta*, and *para N*-alkylpyridylporphyrins share the similar hydrophilicity, the *ortho* isomers are relatively more bulky (when compared to the *para* and *meta* analogues), which may limit to some extent their *in vivo* efficacy. In an *E. coli* experiment [26], the *meta* isomer Mn^{III}TM-3-PyP^{5+}, which is significantly less potent *in vitro* than its *ortho* analogue, showed *in vivo* efficiency comparable to the *ortho* isomer in protecting SOD-deficient *E. coli* to grow aerobically. The planar *para* isomer, while equally able antioxidant as *meta in vitro*, is inferior to the *meta* analogue *in vivo*; we have seen in our *E. coli* model of oxidative stress that the increased interactions of the *para* isomers with nucleic acids introduces toxicity [26]. At the concentration levels where no toxicity of the *meta* isomer is observed, equimolar levels of the para isomer did not allow for the aerobic growth of SOD-deficient *E. coli* in five amino acid medium.

We have shown already that the introduction of bromines onto *β*-pyrrolic positions of Mn^{III}TM-4-PyP^{5+} increases the $E_{½}$ from +60 to 480 mV [12]. That is accompanied by *ca* two orders of magnitude increase in k_{cat} [12]. Herein we synthesized the *meta* analogue, $Mn^{II}Br_8$TM-3-PyP^{4+}, which was fully characterized by uv/vis spectroscopy, elemental analysis, electron spray ionization mass spectrometry, and electrochemistry.

Uv/vis spectroscopy

Spectral properties of $Mn^{II}Br_8$TM-3-PyP^{4+} given in Experimental section are very similar to those of its *para* analogue. The addition of 8 bromines increases electron-deficiency in both isomers, which in turn stabilizes the Mn in its +2 oxidation state. This, in association with the non-planar conformation imposed by the bromines, affects significantly the metal/ligand stability of these brominated compounds (Fig. 2). Both the extent and the rate of demetallation of these complexes are concentration-dependent. At concentrations greater than 10 μM in phosphate buffer (pH 7.8) the complexes are stable for hours, whereas at lower concentrations (*e.g.*, 2 μM; Fig. 2) both complexes ($Mn^{II}Br_8$TM-3-PyP^{4+} and $Mn^{II}Br_8$TM-4-PyP^{4+}) show an initial rapid loss of Mn (~10 min), after which they reach metal/ligand equilibrium and no significant loss of the metal is further observed within hours (Fig. 2c); the demetallation is much faster with *para* than with *meta* isomer (Fig. 2b and 2a, respectively). This behavior is not altered by the presence or absence of excess chloride, which is of importance for the measurements of the kinetic salt effects on k_{cat}. Of note, both Mn porphyrins are stable for days at mM concentration in the phosphate buffer (pH 7.8). Slightly less positive $E_{1/2}$ of the *meta* isomer than of the *para* analogue (Table 1) indicates a less electron-deficient metal center, resulting in a more stable *meta* metal/ligand complex.

We are routinely studying the reducibility of Mn porphyrins with cellular reductants because they can possibly act *in vivo* as superoxide reductases, rather than superoxide dismutases [2, 11,27]. While the stabilization of the Mn +2 oxidation state in β-octabrominated *meso N*-methylpyridylporphyrins precludes the assessment of their reducibility, the highly positive $E_{1/2}$ indicates that outstandingly electron-deficient systems will be much more readily reduced (once oxidized) that Mn porphyrins that are stable in +3 oxidation state, as is MnTE-2-PyP^{5+}.

Electrochemistry

The voltammogram of the Mn complex $Mn^{II}Br_8TM\text{-}3\text{-}PyP^{4+}$ shows a reversible process associated with the Mn^{III}/Mn^{II} redox couple with $E_{½}$ = +468 mV *vs* NHE (Fig. 3a), whereas the irreversible process with $E_{½}$ = +122 mV *vs* NHE (Fig. 3b) was observed in the voltammogram of the brominated free-base porphyrin. The metal-centered reduction potential of the Mn porphyrin complex and the ring-centered reduction potential of the free-base porphyrin are similarly affected by the bromination of the pyrrolic positions. An anodic shift of 418 mV for the metal-centered process in $Mn^{II}Br_8TM\text{-}3\text{-}PyP^{4+}$ (as compared to that of $Mn^{III}TM\text{-}3\text{-}PyP^{5+}$) was observed (Table 1) and such shift of 52 mV/Br is comparable to that reported for other β-brominated Mn porphyrins [12,43-45]. Likewise, the introduction of bromine atoms on the β-pyrrole positions of metal-free ligand, $H_2TM\text{-}3\text{-}PyP^{4+}$ resulted in an anodic shift in the reduction potential by 334 mV (*i.e.*, 42 mV/Br, Table 1). Worth noting is that the reduction potential of $HBr_8TM\text{-}3\text{-}PyP^{3+}$ is 70 mV more positive than that of the non-brominated Mn complex, $Mn^{III/II}TM\text{-}3\text{-}PyP^{5+/4+}$ ($E_{½}$ = +52 mV *vs* NHE, Table 1). That suggests that the brominated free-base porphyrin itself may be able to catalyze $O_2^{\bullet-}$ dismutation. No change in the reduction potential of $Mn^{II}Br_8TM\text{-}3\text{-}PyP^{4+}$ in 0.05 M phosphate buffer (pH 7.8) was observed by increasing the ionic strength with either NaCl or phosphate buffer, which is of relevance to the kinetic salt effect measurements (see below); this suggested no chloride binding in 0.05 M phosphate buffer.

SOD activity (cytochrome c assay)

The higher metal/ligand stability of the brominated *meta* isomer $Mn^{II}Br_8TM\text{-}3\text{-}PyP^{4+}$ (Fig. 2) allowed an easier assessment of its SOD-like activity as compared to its *para* analogue. In our previous work on $Mn^{II}Br_8TM\text{-}4\text{-}PyP^{4+}$, however, the initial rapid loss of Mn (reported herein) to yield an "equilibrated" solution was not accounted for. Given the extent of demetallation and the rapid nature of this process with brominated *para* isomer, it is essentially very difficult under our experimental conditions to obtain a k_{cat} that could accurately reflect the actual concentration of the Mn complex at nM conditions. The previously reported rate constant of log k_{cat} = 8.34 corresponds to the situation where no demetallation was assumed; it represents, thus, the lower limit for k_{cat} for $Mn^{II}Br_8TM\text{-}4\text{-}PyP^{4+}$. If a minimum 30% loss of Mn is value for Mn^{II} considered, as suggested by the data in Fig. 2, an estimated log k_{cat} $Br_8TM\text{-}4\text{-}PyP^{4+}$ is > 8.67.

With the brominated *meta* isomer the situation is better defined as this compound is considerably more stable towards demetallation than its *para* analogue (Fig. 2). Assuming that no demetallation occurs, the log k_{cat} measured for $Mn^{II}Br_8TM\text{-}3\text{-}PyP^{4+}$ is 8.80. Given that the loss of Mn^{2+} is ~10% during first several minutes (Fig. 2c), the log k_{cat} is estimated to be at least 8.85 which is essentially identical to the k_{cat} for the SOD enzymes [25–27] (Table 2). Thus, the bromination of $Mn^{III}TM\text{-}3\text{-}PyP^{5+}$ to yield $Mn^{II}Br_8TM\text{-}3\text{-}PyP^{4+}$ increased the catalytic rate constant by ~160-fold. The data are summarized in Table 2.

Kinetic salt effect

The kinetic salt effect (KSE) was determined as previously described [2,3]. In all cases where the reaction of cationic porphyrins with anionic superoxide was studied an increase in ionic strength resulted in a decrease in k_{cat}, the effect being much less pronounced with *meta* and *para* isomers than with *ortho* isomers [2,3]. In a phosphate buffer of different concentrations (*i.e.*, ionic strength), a small positive kinetic salt effect on the k_{cat} values for $Mn^{II}Br_8TM\text{-}3\text{-}PyP^{4+}$ was observed. Surprisingly, however, when NaCl was used to adjust the ionic strength, an increase in ionic strength resulted in a significant increase in k_{cat} for this *meta* isomer (Fig. 4). For the brominated *para* isomer $Mn^{II}Br_8TM\text{-}4\text{-}PyP^{4+}$, a positive KSE was also observed, but to a smaller extent than that found for its *meta* counterpart. For the non-brominated *meta* and *para* Mn porphyrins [2,3] (Fig. 4), a negative KSE indicated that the species of opposite

charge are involved in the dismuting rate-limiting step; the small value of KSE shows that the electrostatics contributes very little to the catalytic rate constant of these complexes. This implies that the charges of the *meta* and *para* pyridinium moieties are considerably far away from the active site (Mn center) to provide suitable electrostatic facilitation for the superoxide dismutation. With brominated complexes, however, the positive KSE observed implies that species of similar charges are involved in the dismuting rate-limiting step, *i.e.* there is an overall negative electronic density nearby the Mn center in the brominated Mn complexes. A first hypothesis considered to explain the increase in electronic density near the Mn site was the one that invokes an axial coordination of chloride/phosphate to the Mn center, which would increase the formal charge on the Mn. The binding of Cl^- would be expected to affect both $E_{½}$ and the stability of the Mn complex, but neither was corroborated experimentally, *i.e.*, no change in $E_{½}$ or rate of Mn loss was observed as the chloride concentration increased. This suggests that the KSE for the brominated Mn complexes relates not to a change in the first but in the second coordination sphere, which has been documented for the free-base H_2TM-4-PyP^{4+} [46]. An increased ion-pairing of the anion (phosphate and/or chloride) in a close proximity to the brominated porphyrin core [46] would result in an overall negative charge density near the Mn center and, thus, in a positive KSE. It is worth noting that the KSE for $Mn^{II}Br_8$TM-3-PyP^{4+} is considerably greater than that of $Mn^{II}Br_8$TM-4-PyP^{4+}, which is consistent with the closer proximity of the quaternary nitrogens of the *meta* isomer to the metal center than that of the *para* isomer. To the best of our knowledge this is the first report on the positive KSE when cationic porphyrins encountered anionic species.

Protection of aerobic growth of SOD-deficient E. coli

We have adopted the growth of SOD-deficient *E. coli* in the restricted five amino acids-medium as a reliable tool for evaluating the ability of a MnP to substitute for SOD. In all previous studies the data obtained with *E. coli* parallel the trends obtained in *in vivo* animal model studies [1–5,11–28,37]. Here we compare the effect of $Mn^{II}Br_8$TM-3-PyP^{4+}, its metal-free porphyrin HBr_8TM-3-PyP^{3+}, and the *para* analogue $Mn^{II}Br_8$TM-4-PyP^{4+} on the aerobic growth of an SOD-deficient *E. coli* strain. The fairly low metal-ligand stability of these Mn porphyrins allow for metal loss during *E. coli* growth. To account for such an event we have compared the effect of Mn porphyrins on *E. coli* growth to that of $MnCl_2$. Mn^{III}TM-2-PyP^{5+} (or ethyl analogue, Mn^{III}TE-2-PyP^{5+}) is usually used as a positive SOD-active control compound in most of our studies [2,4]. We show here (Fig. 5) that the high k_{cat} of the *meta* *β*-brominated Mn(II) porphyrin $Mn^{II}Br_8$TM-3-PyP^{4+} allows it to be extremely effective at nM levels and offer full protection up to 1 μM concentration. At the concentration range used, $MnCl_2$ is hardly protective, indicating that $Mn^{II}Br_8$TM-3-PyP^{4+} indeed acts in its own right as an SOD mimic or as a carrier of Mn into the cell in a similar fashion as suggested for $Mn^{III}Br_8TSPP^{3-}$ [4]. The same may be true for the brominated metal-free ligand HBr_8TM-3-PyP^{3+}. It is less efficient as an SOD mimic in its own right, due to the lower k_{cat}; however *β*-octabrominated metal-free porphyrins are severely distorted and well known for their ability to coordinate metals promptly at room temperature under neutral pH [12,30,44]. HBr_8TM-3-PyP^{3+} can thus readily complex metal from medium *in situ*, whereby acting in the same way as Mn^{II} Br_8TM-3-PyP^{4+}. Both Mn^{II} Br_8TM-3-PyP_{4+} and HBr_8TM-3-PyP^{3+} are toxic at high levels, which may be due to the presence of bromines and/or the scavenging of metals that are essential for *E. coli* growth. The *para* *β*-brominated Mn(II) porphyrin $Mn^{II}Br_8$TM-4-PyP^{4+} is less effective at protecting SOD-deficient *E. coli* than its *meta* isomer, which is consistent with the lower metal/ligand stability of the *para* isomer. We further showed that the *para* isomer is more toxic than its *meta* analogue which is presumably due to the lesser hindrance of the peripheral *para N*-methylpyridyl groups, resulting in increased, yet unfavorable/toxic interactions with nucleic acids [26]. It may thus be that the lower efficacy of $Mn^{II}Br_8$TM-4-PyP^{4+} at ≤ 500 nM compared to its m*eta* analogue, $Mn^{II}Br_8$TM-3-PyP^{4+} is at least in part due to its higher toxicity. At concentration levels where brominated porphyrins are protective Mn^{III}TM-2-PyP^{5+} is ineffective, which is consistent with

our previous data that full protection is obtained at ~ 20 μM [26]. Our data indicate that the size of the molecule did not have a significant impact on the ability of the compound to substitute for SOD in *E. coli*. The same has been observed with fairly big lipophilic hexyl porphyrin, Mn^{III}TnHex-2-PyP^{5+} (log k_{cat} = 7.48) [24], which was also able to protect SOD-deficient *E. coli* at submicromolar levels.

In conclusions, a manipulation of the electron-deficiency of a cationic porphyrin resulted in the highest k_{cat} ever reported for a metalloporphyrin, being essentially identical to the k_{cat} of superoxide dismutases. Our data show that such high thermodynamic and kinetic facilitation, which leads to an exceptionally high k_{cat} for the $O_2^{\bullet -}$ disproportionation, can be achieved not only with an N_5-type coordination motif, as rationalized previously for aza crown ether (cyclic polyamines) complexes [47-49], but also with a N_4-type motif as in the Mn porphyrin case. Interestingly, both aza crown ethers and β-octabrominated porphyrins [12] share a common alternating “up-down-up-down” steric arrangement of the nitrogens around the Mn center, which is presumably critical for the dismutation process [47–49]. Thus, future work on molecules that possess appropriate geometries for efficacious catalysis is highly justifiable.

Acknowledgements

JSR and IBH acknowledge the support by the National Institutes of Health (IR21-ESO/3682) and the National Institutes for Allergy and Infectious Diseases (U19AI067798) grants. GDS and YMI acknowledge the research grants of the Brazilian Research Council (CNPq) and the Fundação do Amparo à Pesquisa do Estado de Minas Gerais (FAPEMIG). IS thanks NIH/NCI Duke Comprehensive Cancer Center Core Grant (5-P30-CA14236-29). LB acknowledges grant MB07/04 from Kuwait University. The excellent technical assistance of Fatima Sequeira and Milini Thomas is acknowledged.

Abbreviations

Meso
: refers to the substituents at the 5,10,15, and 20 positions (*meso* carbon) of the porphyrin

β
: refers to the substituents at the 2,3,7,8,12,13,17, and 18 positions (*β*-pyrrole carbons) of the porphyrin

cyt *c*
: cytochrome *c*

DMF
: *N*,*N*-dimethylformamide

EDTA
: sodium salt of ethylenediaminetetracetic acid

ESI
: electrospray ionization

H_2P^{4+} and HP^{3+}
: any metal free porphyrin (di and monoprotonated)

H_2TM-3-PyP^{4+}
: *meso*-tetrakis(*N*-methylpyridinium-3-yl)porphyrin

H_2TM-4-PyP^{4+}
: *meso*-tetrakis(*N*-methylpyridinium-4-yl)porphyrin

$Cu^{II}TM\text{-}3\text{-}PyP^{4+}$
copper(II) *meso*-tetrakis(*N*-methylpyridinium-3-yl)porphyrin

$Cu^{II}Br_8TM\text{-}3\text{-}PyP^{4+}$
copper(II) *β*-octabromo-*meso*-tetrakis(*N*-methylpyridinium-3-yl)porphyrin

$HBr_8TM\text{-}3\text{-}PyP^{3+}$
β-octabromo-*meso*-tetrakis(*N*-methylpyridinium-3-yl)porphyrin

$Mn^{II}Br_8TM\text{-}3\text{-}PyP^{4+}$
manganese(II) *β*-octabromo-*meso*-tetrakis(*N*-methylpyridinium-3-yl)porphyrin

$Mn^{II}Br_8TM\text{-}4\text{-}PyP^{4+}$
manganese(II) *β*-octabromo-*meso*-tetrakis(*N*-methylpyridinium-4-yl)porphyrin

$Mn^{III}Br_8T\text{-}2\text{-}PyP^{+}$
manganese(III) *β*-octabromo-*meso*-tetrakis(2-pyridyl)porphyrin

$Mn^{III}TE\text{-}2\text{-}PyP^{5+}$
manganese(III) *meso*-tetrakis(*N*-ethylpyridinium-2-yl)porphyrin

$Mn^{III}TM\text{-}2\text{-}PyP^{5+}$
manganese(III) *meso*-tetrakis(*N*-methylpyridinium-2-yl)porphyrin

$Mn^{III}TM\text{-}3\text{-}PyP^{5+}$
manganese(III) *meso*-tetrakis(*N*-methylpyridinium-3-yl)porphyrin

$Mn^{III}TM\text{-}4\text{-}PyP^{5+}$
manganese(III) *meso*-tetrakis(*N*-methylpyridinium-4-yl)porphyrin

$Mn^{III}TnHex\text{-}2\text{-}PyP^{5+}$
manganese(III) *meso*-tetrakis(*N*-n-hexylpyridinium-2-yl)porphyrin

$[Mn^{III}Br_8TSPP]^{3-}$
manganese(III) *β*-octabromo-*meso*-tetrakis(4-sulfonatophenyl)porphyrin; metal-free ligand denotes same species as free-base porphyrin

IC_{50}
concentration that causes 50% inhibition of cytochrome *c* reduction by $O_2^{\bullet-}$

MS
mass spectrometry

NHE
normal hydrogen electrode

SAR
structure-activity relationship

SOD
superoxide dismutase

References

1. Batini-Haberle I, Benov L, Spasojevi I, Hambright P, Crumbliss AL, Fridovich I. Inorg Chem 1999;38:4011–4022.
2. Rebouças JS, Spasojevi I, Tjahjono DH, Richaud A, Mendez F, Benov L, Batini-Haberle I. Dalton Trans 2008:1233–1242. [PubMed: 18283384]

3. Spasojevi I, Batini-Haberle I, Rebouças JS, Idemori YM, Fridovich I. J Biol Chem 2003;278:6831–6837. [PubMed: 12475974]
4. Rebouças JS, DeFreitas-Silva G, Spasojevi I, Idemori YM, Benov L, Batini-Haberle I. Free Radical Biol Med. 200810.1016/j.freeradbiomed.2008.04.009
5. Reboucas JS, Spasojevi I, Batini-Haberle I. J Biol Inorg Chem 2008;13:289–302. [PubMed: 18046586]
6. Ferrer-Sueta G, Vitturi D, Batini-Haberle I, Fridovich I, Goldstein S, Czapski G, Radi R. J Biol Chem 2003;278:27432–27438. [PubMed: 12700236]
7. Coulter AD, Emerson JP, Kurtz DM, Cabelli DE. J Am Chem Soc 2006;122:11555–11556.
8. Batini-Haberle I, Spasojevi I, Fridovich I. Free Radical Biol Med 2004;37:367–374. [PubMed: 15223070]
9. Trostchansky A, Ferrer-Sueta G, Batthyany C, Botti H, Batini-Haberle I, Radi R, Rubbo H. Free Radical Biol Med 2003;35:1293–1300. [PubMed: 14607528]
10. Ferrer-Sueta G, Quijano C, Alvarez B, Radi R. Methods Enzymol 2002;349:23–37. [PubMed: 11912912]
11. Batini-Haberle I, Spasojevi I, Stevens RD, Hambright P, Fridovich I. J Chem Soc, Dalton Trans 2002:2689–2696.
12. Batini-Haberle I, Liochev SI, Spasojevi I, Fridovich I. Arch Biochem Biophys 1997;343:225–233. [PubMed: 9224734]
13. Zhao Y, Chaiswing L, Oberley TD, Batini-Haberle I, St Clair W, Epstein CJ, St Clair D. Cancer Res 2005;65:1401–1405. [PubMed: 15735027]
14. Moeller BJ, Batini-Haberle I, Spasojevi I, Rabbani ZN, Anscher MS, Vujaskovi ž, Dewhirst MW. Int J Rad Oncol Biol Phys 2005;63:545–552.
15. Benov L, Batini-Haberle I. Free Radical Res 2005;38:81–88. [PubMed: 15875815]
16. Sheng H, Spasojevi I, Warner DS, Batini-Haberle I. Neurosci Lett 2004;366:220–225. [PubMed: 15276251]
17. Sheng H, Enghild J, Bowler R, Patel M, Calvi CL, Batini-Haberle I, Day BJ, Pearlstein RD, Crapo JD, Warner DS. Free Radic Biol Med 2002;33:947–961. [PubMed: 12361805]
18. Vujaskovi I, Batini-Haberle ZN, Rabbani Q-F, Feng SK, Kang I, Spasojevi TV, Samulski I, Fridovich Dewhirst MW, Anscher MS. Free Radic Biol Med 2002;33:857–863. [PubMed: 12208373]
19. Piganelli JD, Flores SC, Cruz C, Koepp J, Young R, Bradley B, Kachadourian R, Batini-Haberle I, Haskins K. Diabetes 2002;51:347–355. [PubMed: 11812741]
20. Mackensen GB, Patel M, Sheng H, Calvi CL, Batini-Haberle I, Day BJ, Liang LP, Fridovich I, Crapo JD, Pearlstein RD, Warner DS. J Neurosci 2001;21:4582–4592. [PubMed: 11425886]
21. Aslan M, Ryan TM, Adler B, Townes TM, Parks DA, Thompson JA, Tousson A, Gladwin MT, Tarpey MM, Patel RP, Batini-Haberle I, White CR, Freeman BA. Proc Natl Acad Sci USA 2001;98:15215–15220. [PubMed: 11752464]
22. Bottino R, Balamurugan AN, Bertera S, Pietropaolo M, Trucco M, Piganelli JD. Diabetes 2002;51:2561–2567. [PubMed: 12145171]
23. Sompol P, Ittarat W, Tangpong J, Chen Y, Doubinskaia I, Batini-Haberle I, Mohammad Abdul H, Butterfield A, St Clair DK. Neuroscience. 2007in press
24. Okado-Mastsumoto A, Batini-Haberle I, Fridovich I. Free Radic Biol Med 2004;37:401–410. [PubMed: 15223074]
25. Benov L, Batini-Haberle I, Spasojevi I, Fridovich I. Arch Biochem Biophys 2002;402:159–165. [PubMed: 12051659]
26. Batini-Haberle I, Benov L, Spasojevi I, Fridovich I. J Biol Chem 1998;273:24521–24528. [PubMed: 9733746]
27. Batini-Haberle I, Spasojevi I, Stevens RD, Hambright P, Neta P, Okado-Matsumoto A, Fridovich I. J Chem Soc, Dalton Trans 2004:1696–1702.
28. Batini-Haberle I, Benov L, Fridovich I. Anal Biochem 1999;275:267. [PubMed: 10552917]
29. Waud WR, Brady FO, Wiley RD, Rajagopalan KV. Arch Biochem Biophys 1975;169:695–701. [PubMed: 1180567]
30. Richards RA, Hammons K, Joe M, Miskelly GM. Inorg Chem 1996;33:1940–1944.

31. McCord JM, Fridovich I. J Biol Chem 1969;244:6049–6055. [PubMed: 5389100]
32. Spasojevi I, Batini-Haberle I, Stevens RD, Hambright P, Thorpe AN, Grodkowski J, Neta P, Fridovich I. Inorg Chem 2001;40:726–739. [PubMed: 11225116]
33. Imlay JA, Linn S. J Bacteriol 1987;169:2967–2976. [PubMed: 3298208]
34. Munroe W, Kingsley C, Daruzo A, Gralla EB, Imlay JA, Srinivasan C, Valentine JS. J Inorg Biochem 2007;101:1875–1882. [PubMed: 17723242]
35. Vance CK, Miller AF. J Am Chem Soc 1998;120:461–467.
36. Michel E, Nauser T, Sutter B, Bounds PL, Koppenol WH. Arch Biochem Biophys 2005;439:234–240. [PubMed: 15978540]
37. Goldstein S, Fridovich I, Czapski G. Free Radical Biol Med 2006;41:937–941. [PubMed: 16934676]
38. Lawrence GD, Sawyer DT. Biochemistry 1979;18:3045–3050. [PubMed: 380641]
39. Barrette WC Jr, Sawyer DT, Free JA, Asada K. Biochemistry 1983;22:624–627. [PubMed: 6340720]
40. Faraggi, M. $O_2^{\bullet -}$ Dismutation Catalyzed by Water- soluble Porphyrins: A Pulse Radiolysis Study. Bors, W.; Saran, M.; Tait, D., editors. Walter de Gruyter; Berlin: 1984. p. 419-430.
41. Batini-Haberle I, Spasojevi I, Stevens RD, Bondurant B, Okado-Matsumoto A, Fridovich I, Vujaskovi, Dewhirst MW. Dalton Trans 2006:617–624. [PubMed: 16402149]
42. Kachadourian R, Batini-Haberle I, Fridovich I. Inorg Chem 1999;38:391–396.
43. Ou Z, Shao J, D'Souza F, Tagliatesta P, Kadish KM. J Porphyrins Phthalocyanines 2004;8:201–214.
44. Rebouças JS, de Carvalho MEMD, Idemori YM. J Porphyrins Phthalocyanines 2002;6:50–57.
45. do Nascimento E, deF Silva G, Caetano FA, Fernandes MAM, da Silva DC, de Carvalho MEMD, Pernaut JM, Rebouças JS, Idemori YM. J Inorg Biochem 2005;99:1193–1204. [PubMed: 15833343]
46. Foster N. J Magn Reson 1984;56:140–143.
47. Riley DP, Henke SL, Lennon PJ, Aston K. Inorg Chem 1999;38:1908–1917. [PubMed: 11670965]
48. Aston K, Rath N, Naik A, Slomczynska U, Schall OF, Riley DP. Inorg Chem 2001;40:1779–1789. [PubMed: 11312732]
49. Riley DP. Adv Supramol Chem 2000;6:217–244.

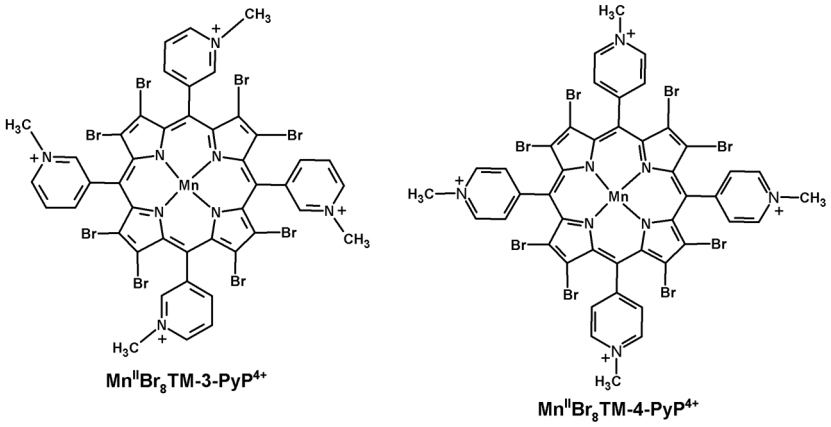

Figure 1.
Schematic structures of the $Mn^{II}Br_8TM\text{-}3\text{-}PyP^{4+}$ and $Mn^{II}Br_8TM\text{-}4\text{-}PyP^{4+}$.

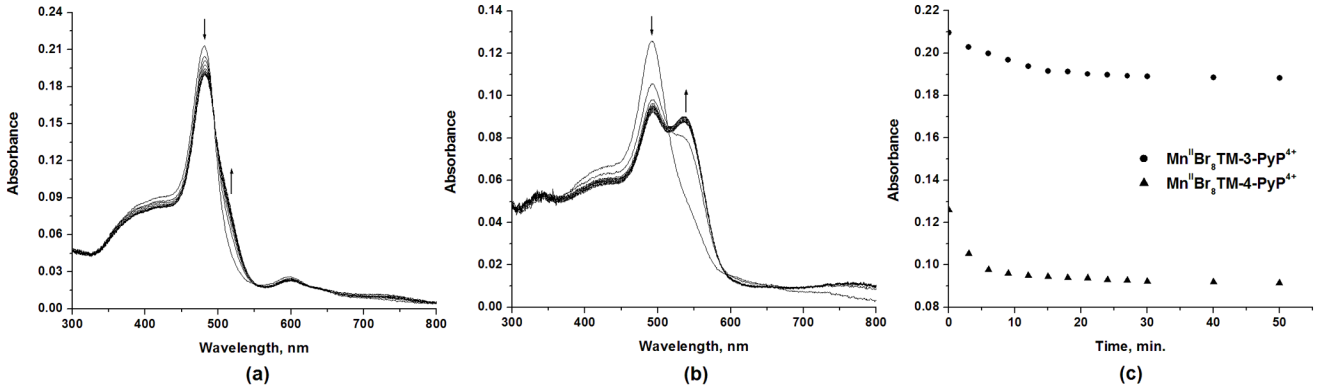

Figure 2.

Partial demetallation of ~2 μM solutions of (a) $Mn^{II}Br_8TM\text{-}3\text{-}PyP^{4+}$ and (b) $Mn^{II}Br_8TM\text{-}4\text{-}PyP^{4+}$ in 0.05 M phosphate buffer (pH 7.8). (c) Decay of the Soret bands of $Mn^{II}Br_8TM\text{-}3\text{-}PyP^{4+}$ (•, 484 nm) and $Mn^{II}Br_8TM\text{-}4\text{-}PyP^{4+}$ (▲, 492 nm) during the demetallation process.

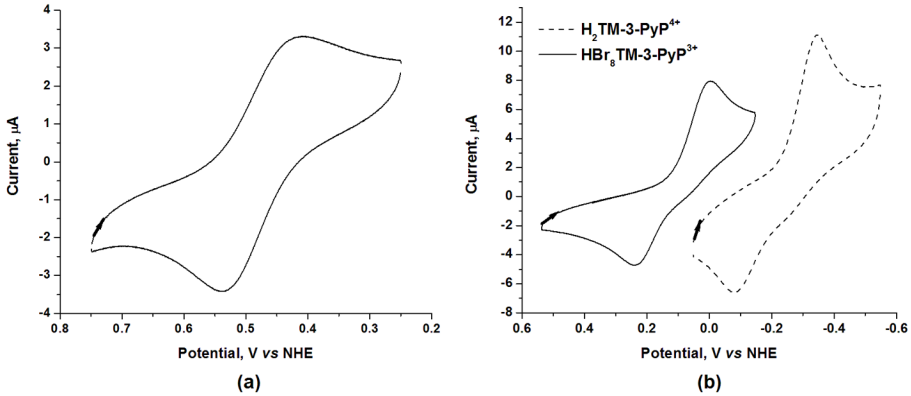

Figure 3.

Cyclic voltamogram of (a) 0.5 mM $Mn^{II}Br_8TM\text{-}3\text{-}PyP^{4+}$ and (b) 0.5 mM $HBr_8TM\text{-}3\text{-}PyP^{3+}$ and 0.5 mM $H_2TM\text{-}3\text{-}PyP^{4+}$. Conditions: 0.05 M phosphate buffer (pH 7.8), 0.1 M NaCl, scan rate 0.1 V s^{-1}.

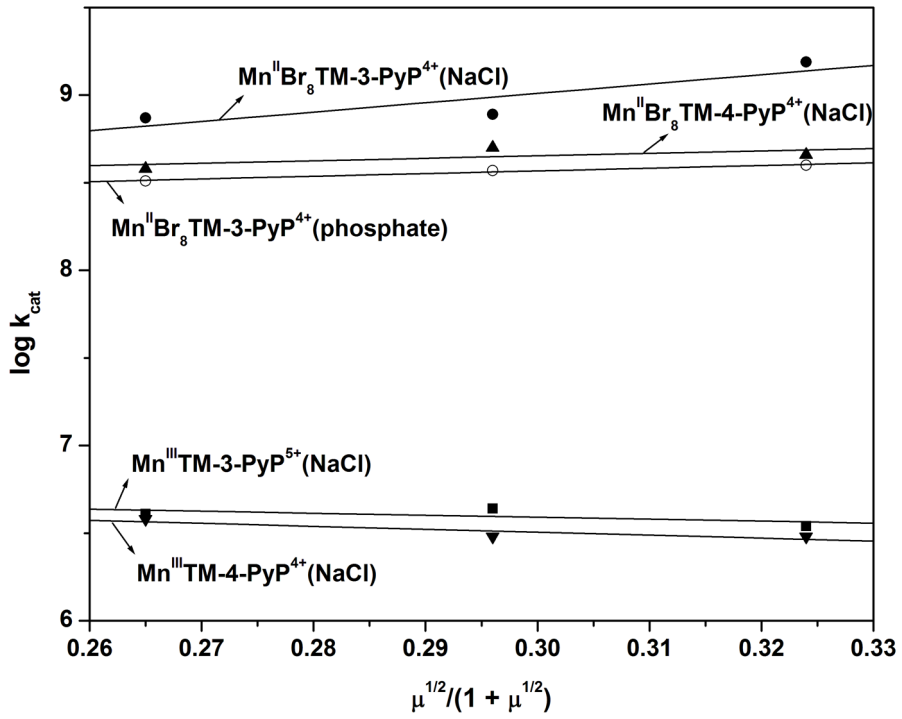

Figure 4.
Kinetic salt effect on the SOD activity of Mn porphyrins. The k_{cat} values were determined by the cyt *c* assay in 0.05 M phosphate buffer, 0.1 mM EDTA at 25 ± 1°C. Ionic strength (μ) adjusted with NaCl (•, ▲, ■, ▼) or phosphate (○).

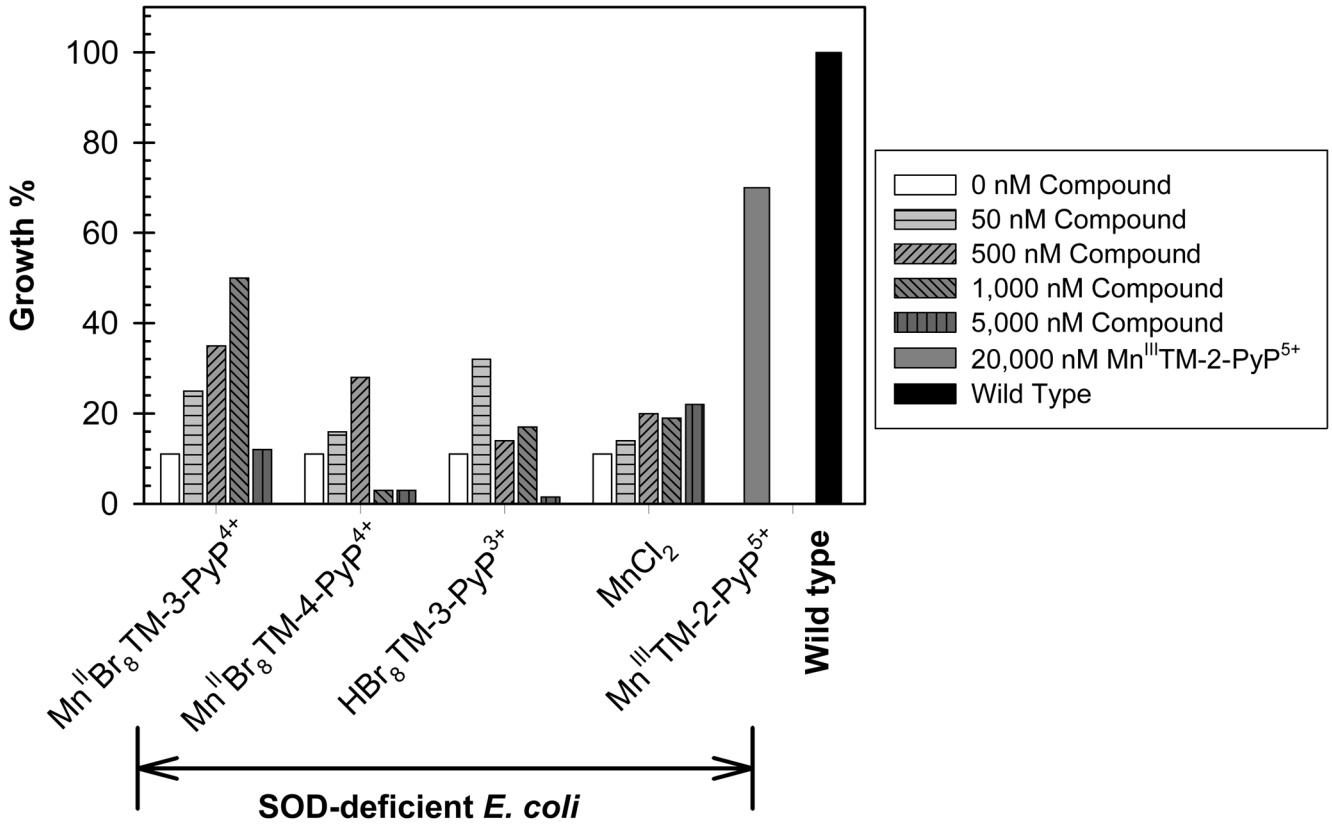

Figure 5.

Aerobic growth of SOD-deficient *E. coli* JI132 strain in the presence or absence of porphyrins or $MnCl_2$ (at 50, 500, 1000 or 5000 nM) in 5AA medium at the 13th hour. Readings were taken at 700 nm. Although "HBr_8TM-3-PyP^{3+}" was added to the medium as the metal-free porphyrin, the protective effect of this compound maybe at least in part due to its ability to complex Mn from the medium (see text). Aerobic growth of the wild type *E. coli* AB1157 was used as control.

Table 1

Electrochemical data for free-base porphyrins and their Mn complexes in aqueous solutions[a]

Porphyrins	$E_{½}$, mV *vs* NHE	Ref.
H_2TM-3-PyP^{4+}	−212[b] (268)[c]	this work
Mn^{III}TM-3-PyP^{5+}	+52	[26]
HBr_8TM-3-PyP^{3+}	+122[b] (233)[c]	this work
Mn^{II} Br_8TM-3-PyP^{4+}	+468 (93)[c]	this work
Mn^{III}TM-4-PyP^{5+}	+60[d]	[26]
Mn^{II} Br_8TM-4-PyP^{4+}	+480	[12]
Cu,Zn-SOD	*ca*. +300	[35–37]

[a] Conditions: 0.5 mM porphyrin, 0.05 M phosphate buffer, pH 7.8, 0.1 M NaCl, scan rate 0.1 V s^{-1}.

[b] Irreversible wave.

[c] Cathodic/anodic peak-to-peak separation.

Table 2

SOD-like activity of the porphyrins studied.[a]

Porphyrin	IC_{50}, M[b]	log k_{cat}[c]	Ref.
Mn^{III}TM-3-PyP^{5+}	6.5×10^{-7}	6.61	[26]
$Mn^{II}Br_8$TM-3-PyP^{3+}	$\leq 3.7 \times 10^{-9}$	≥8.85	this work
Mn^{III}TM-4-PyP^{5+}	6.7×10^{-7}	6.58	[26]
$Mn^{II}Br_8$TM-4-PyP^{4+}	$\leq 5.6 \times 10^{-9}$	≥8.67	this work
Cu,Zn-SOD	1.3×10^{-9}	ca. 9	[35–37]

[a] Conditions: 0.05 M phosphate buffer, 0.10 mM EDTA, pH 7.8, 40 μM xanthine, ~ 10 μM cytochrome *c*.

[b] IC_{50} is the concentration of compound that causes a 50% inhibition of the cyt *c* reduction by $O^{\bullet -}$. The errors in IC_{50} are within 10%.

[c] Error of ± 10 %.